Journal of Power Sources 227 (2013) 35–40

Contents lists available at SciVerse ScienceDirect

Journal of Power Sources

journal homepage: www.elsevier.com/locate/jpowsour

Fabrication of structured anode-supported solid oxide fuel cell by powder injection molding

Antonin Faes [a,1], Hervé Girard [a], Amédée Zryd [a], Zacharie Wuillemin [b], Jan Van herle [c,*]

[a] Design and Materials Unit, University of Applied Science Western Switzerland, Route du Rawyl 47, CH-1950 Sion, Switzerland
[b] HTceramix–SOFCpower, Avenue des Sports 26, CH-1400 Yverdon-les-Bains, Switzerland
[c] Laboratory of Industrial Energy Systems (LENI), Ecole Polytechnique Fédérale de Lausanne (EPFL), CH-1015 Lausanne, Switzerland

HIGHLIGHTS

- First electrochemical test of planar structured anode-supported SOFC produced by PIM.
- Multifunctional parts for SOFC stack: (1) gas diffusion layer + (2) structured anode-support.
- High production rate and high tolerance PIM process for low cost SOFC complex parts.
- Good performance and low degradation confirm the proof-of-concept before upscaling.

GRAPHICAL ABSTRACT

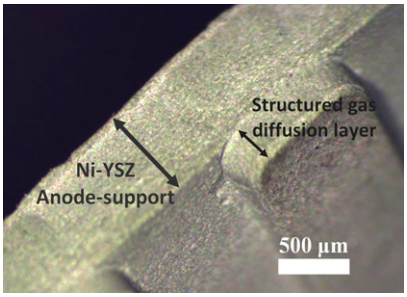

ARTICLE INFO

Article history:
Received 1 September 2012
Received in revised form
9 October 2012
Accepted 3 November 2012
Available online 16 November 2012

Keywords:
Ceramic powder injection molding
PIM
CIM
Solid oxide fuel cells
SOFC
Structured anode-supported cells

ABSTRACT

Powder Injection Molding (PIM) gives the possibility to produce, at an industrial rate, ceramic parts with fine details. It is thus a possible approach to reduce the fabrication costs of Solid Oxide Fuel Cells (SOFCs). This work presents fabrication and electrochemical characterization results of injection-molded structured anode-supported SOFCs.

Planar anode-supported SOFCs with fine details have been produced by injection molding of a mixture of nickel oxide (NiO) and yttria-stabilized zirconia (YSZ). The channeling structure and support porosity ensure gas transport on the fuel side. Initial anode support characterizations like sintering shrinkage, porosity and electrical conductivity have been done on simple Ni–YSZ test bars. Thin YSZ electrolyte has been deposited by spin-coating on the PIM green body before half-cell co-sintering.

Electrochemical testing was carried out with a lanthanum–strontium manganite (LSM)–YSZ cathode. The performance is comparable to tape-cast anode-supported cells, with 0.45 W cm^{-2} obtained at 0.6 V and 810 °C. Medium-term galvanostatic testing shows a degradation rate of about 1.1% kh^{-1}. Post-test analysis with scanning electron microscopy (SEM) and energy dispersive X-ray spectroscopy (EDS) attribute this mainly to cathode degradation due to Cr and S poisoning. These results are therefore promising for using a PIM fabrication process in the SOFC field.

1. Introduction

Solid oxide fuel cells (SOFCs) are a promising technology for the conversion of chemical energy into electrical energy and heat (co-generation). Their electrical efficiency from primary fuels is unbeatable especially for small systems (1 kW). But their entrance

* Corresponding author. EPFL-STI-IGM-LENI, MEA2-392, Station 9, CH-1015 Lausanne, Switzerland. Tel.: +41 21 693 55 10; fax: +41 21 693 35 02.
E-mail address: jan.vanherle@epfl.ch (J. Van herle).
[1] Present address: CSEM SA, PV Center, Rue Jaquet-Droz 1, CH-2002 Neuchâtel, Switzerland.

0378-7753/$ – see front matter © 2012 Elsevier B.V. All rights reserved.
http://dx.doi.org/10.1016/j.jpowsour.2012.11.016

in the market is limited by their actual excessive price and limited lifetime.

Powder injection molding (PIM) can be a solution to reduce the costs of SOFC. It allows the production of complex 3D designs with near net shape at an industrial rate, in metallic, ceramic or composite materials. During the PIM process, the raw powder is mixed with polymer binders to produce a feedstock, which is then processed with an injection molding press. The green parts (as-injected) can be handled and adjusted if needed before chemical and/or thermal debinding to remove the polymers. The brown part (after debinding) is sintered to obtain final dimension and properties. The homogeneity of injection-molded parts is higher than for uniaxial pressing, and their final dimensions after sintering shrinkage well controlled [1].

Recently, PIM has been applied in the field of SOFC to produce yttria-stabilized zirconia (YSZ) parts [2] and NiO–YSZ anodes in various shapes [3–9]. These works reported about the feedstock optimization and characterization (formulation, viscosity and mixing behavior), the debinding behavior and the sintered and reduced parts characterization (shrinkage, porosity, conductivity, microstructure and bulk impedance spectroscopy). Xiao et al. recently presented an electrochemical test of cone-shaped tubular anode-supported SOFC produced by a low-pressure injection molding technique. With an 8YSZ dip-coated electrolyte and an LSM–YSZ cathode, maximal power densities of 0.5 and 0.8 W cm^{-2} were reached at 800 °C and 850 °C, respectively [7].

In this work, PIM is used to produce anode supports with a finely corrugated structure which will be in contact with the metal interconnect and will allow a proper gas distribution on the anode side. This structured anode-support will also fulfill the function of gas diffusion layer (GDL). The saving of one part on the single repeat element unit (SRU) will be multiplied on the full stack and will help solving other compatibility problems of the GDL layer with the anode and the interconnect such as thermal expansion coefficient differences or high-temperature solid state reaction. Finally, it will simplify the stack assembly and reduce the total cost of the 'hot box' zone.

This work demonstrates the feasibility of an SOFC single repeat element with PIM components and reports about the injection process, the cell fabrication, the electrochemical and degradation tests.

2. Experimental procedure

2.1. Materials

The materials used for the anode are NiO powder (Green Nickel Oxide standard grade, Novamet Specialty Products Corp., Wyckoff, USA) and Zirconia stabilized with 8 mol% Yttria, 8YSZ (MELox 8YF, MEL Chemicals, Manchester, UK). The particles are agglomerated and the size of the agglomerates varies between 14–18 μm for the NiO and 0.5–1 μm for the 8YSZ.

2.2. Feedstock formulation and preparation

The proportions of NiO and YSZ are 58 and 42 wt% respectively, according to Cologna et al. [10]. A feedstock was prepared by mixing these powders in a Coperion LUK 1.0 sigma blade mixer (Werner & Pfleiderer, Stuttgart, Germany) during 2 h at 140 °C, using as binders paraffin wax (PW purum; pellets, Sigma–Aldrich Chemie GmbH, Buchs, Switzerland), stearic acid (SA, Fluka purum; >97%, Sigma–Aldrich Chemie GmbH, Buchs, Switzerland) and low density polyethylene (LDPE Riblene MP30; Polimeri Europa, San Donato Milanese, Italy) in proportions given in Table 1. Granulation was performed by cooling down and crushing the mixture by slow shearing.

Table 1
Feedstock formulation for the NiO–8YSZ ceramic powder.

Component	Powder		Binder		
	NiO	8YSZ	LDPE	SA	PW
vol%	30.4	24.6	15.7	4.5	24.8
vol% global	55.0		45.0		

2.3. Powder injection molding

Simple test bars (5 × 5 × 40 mm) and structured anode-support disks of 40 mm in diameter and 0.5–1 mm in thickness were injection molded in an Arburg 221K 350-100 machine (Arburg GmbH + Co KG, Lossburg, Germany). The mold temperature was controlled at 40°C ± 1 °C. Injection molding of the anodes was performed in a partial vacuum to improve the filling of the details, with a flow rate and an injection pressure of 15 cm^3 s^{-1} and 1500 bar, respectively.

2.4. Porosity, dilatometry and electrical conductivity of the anode-support

The porosity was measured by the Archimedes method on as-sintered test bar samples after sintering 1 h at 1150, 1250, 1350 and 1450 °C under air (Nabertherm HT 16/17, Nabertherm GmbH, Lilienthal, Germany). The thermal characteristics of this feedstock, as well as of the sintered and reduced components, were assessed by dilatometry, in air, heating rate 10 °C min^{-1} (DIL 402E Netzsch Gerätebau GmbH, Selb, Germany). The four points resistivity method was used to obtain room temperature electrical conductivity of the test bar samples (after reduction 12 h at 800 °C under pure H_2).

2.5. Electrolyte deposition and co-sintering of the structured anode-support

The electrolyte deposition on the anode was done by spin-coating after mechanical polishing of the unstructured sample surface and a heptane debinding step (24 h at 50 °C) to dissolve the paraffin wax and the stearic acid. To prepare the slurry, the same 8YSZ powder, with water and dispersant (Darvan 821A, R.T. Vanderbilt Inc., USA) was milled 2 h 30 m in a Turbula mixer with zirconia balls. An acrylic binder (Duramax B1000, Rohm et Haas, France) was added and the slurry stirred during 30 min before spin-coating at 1300 rpm during 1 min.

To obtain a dense electrolyte, the final thermal debinding and co-sintering of the electrolyte and the support was performed by heating in a high-temperature sintering oven with a heating rate of 2 °C min^{-1}, and three plateaus (1 h each at 200 °C and 500 °C and 2 h at 1450 °C).

2.6. Cathode deposition and contacting layers

The cathode was prepared in the way described in Ref. [11], with a ratio of 50:50 vol.% of LSM ($(La_{0.75}Sr_{0.25})_{0.95}MnO_{3-d}$, Praxair, Inc., USA) and 8YSZ (Tosoh Corp., Japan). An ink was obtained by adding 3.2 wt% of ethylcellulose in terpineol (powder–solvent ratio 1.36). The cathode was deposited by screen-printing. Two layers of LSM/YSZ were deposited before firing 1 h at 1050 °C. A current collection layer of LSC ($La_{0.5}Sr_{0.5}CoO_{3-x}$, Praxair, Inc.) was screen-printed on top of the LSM/YSZ fired cathode. The final cathode size was 1.0 ± 0.1 cm^2 and taken as active cell area.

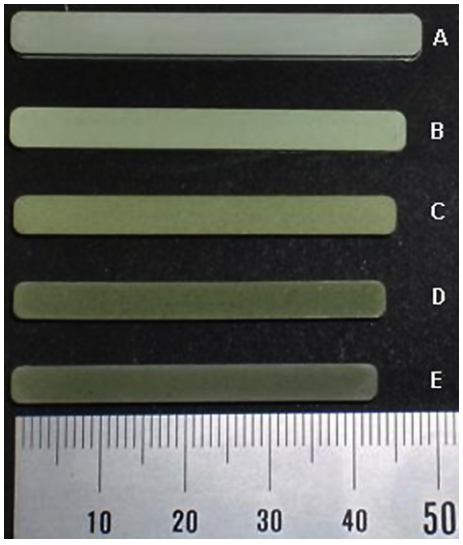

Fig. 1. Injection molded bars in various states: A: green body, from B to E, as-sintered, at respectively 1150 °C, 1250 °C, 1350 °C and 1450 °C. The scale is in mm. (For interpretation of the references to colour in this figure legend, the reader is referred to the web version of this article.)

Finally, an anode current collection layer composed of 90 wt% NiO + 10 wt% YSZ was deposited with a brush on the structured anode-support side.

2.7. Cell testing

The cells were connected with gold and nickel meshes to the cathode and the anode, respectively. The temperature was controlled initially by a K-thermocouple (K-TC1) inserted via the cell side (and so going through the post-combustion zone) but this overestimates the cathode temperature. Then a second K-TC2 is introduced via the air tube and placed nearby the cathode, the temperatures difference between K-TC1 and K-TC2 was about 150 °C. The cell was mounted between two alumina felts in a metallic setup pressed with calibrated springs. The gases arrived at the center of the cell with 450 ml min^{-1} of air for the cathode and 300 ml min^{-1} of humidified hydrogen (around 3% H_2O) for the anode. The gases were post-combusted around the cells. Polarization of the cells was done in galvanostatic mode with an AMEL 555B potentiostat–galvanostat. Measurements were done in a four-wire configuration. Current–voltage curves were taken with an Eco Chemie Autolab® apparatus. Cell testing was done initially at 670 °C during 150 h with a current density of 0.1 A cm^{-2}, due to temperature control using K-TC1. The temperature was then set to 810 °C and the current density to 0.2 A cm^{-2} for the rest of the test.

Table 2
Shrinkage during sintering, as-sintered porosity and room temperature electrical conductivity (after reducing the sample 12 h at 800 °C under H_2) of the injected bars, for various sintering temperatures.

Sintering temperature (°C)	Shrinkage after sintering (%)	Porosity after sintering (%)	Electrical conductivity @ RT (S cm^{-1})
1150	4.2	44	92
1250	7.4	36	1375
1350	10.4	29	3012
1450	12.3	21	4282

2.8. Microstructure observations and energy dispersive X-ray spectrometry

A Leo 1525 scanning electron microscope equipped with a Schottky field emission gun, a Zeiss Gemini column and an Oxford EDS 7426 with a 10 mm^2 Si(Li) detector was used for the microstructure and the EDS analysis. To avoid a charging effect of the non-conductive oxide, samples were coated with a 15 nm thick Pt layer deposited by Ar plasma sputtering (60 s, 40 mA, 1 kV, $5 \cdot 10^{-2}$ mbar on BAL-TEC SCD 050 Sutter Coater).

3. Results and discussion

The green bodies (as-injected) and sintered at different temperatures are presented in Fig. 1 and the fine details of the structured anode are shown in Fig. 2. The height and the width of the fine pattern is 0.5 mm. The linear shrinkage, measured on the bars after sintering, is varying between 4% for a sintering temperature of 1150 °C and 12% at 1450 °C (see Fig. 1 and Table 2). The as-sintered porosity diminishes from 44% to 21% when increasing sintering temperature from 1150 °C to 1450 °C, whereas the electrical conductivity increases at the same time from 90 to more than 4000 S cm^{-1} (Table 2).

The dilatometric study of the green specimen clearly shows the debinding stages (Fig. 3). The first, at around 150 °C, is due to the elimination of incompletely dissolved wax and stearic acid. The second, at 500 °C, corresponds to the thermal degradation of the

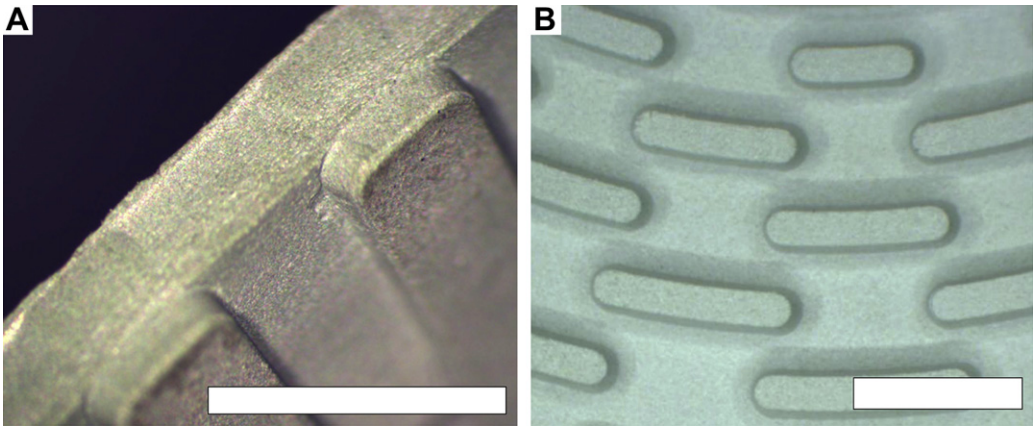

Fig. 2. Pictures of the structured NiO–YSZ anode-support with details of the (a) side and (b) surface of the green parts. The width and height of the fine structured surface are 0.5 mm (left). Both scale bars are 2 mm long. (For interpretation of the references to colour in this figure legend, the reader is referred to the web version of this article.)

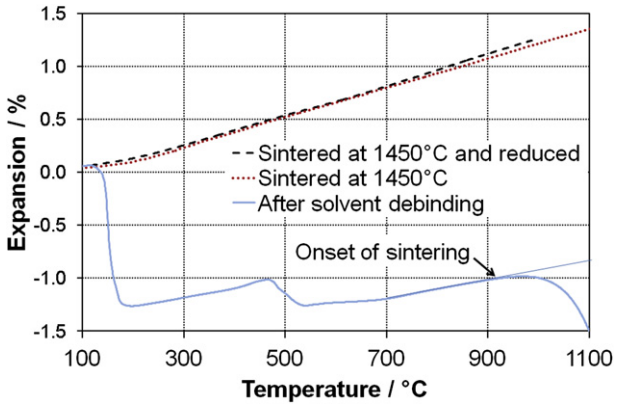

Fig. 3. Expansion versus temperature in air for test bar samples (1) after solvent debinding (in blue), (2) after sintering 1 h at 1450 °C in as-sintered state (in red) and (3) in reduced state (in green, reduction 12 h at 800 °C under H_2). (For interpretation of the references to colour in this figure legend, the reader is referred to the web version of this article.)

LDPE. Finally the onset of sintering is visible around 900 °C. At 1300 °C, the sintering shrinkage is 9% and corresponds to the value observed during normal oven sintering. An average coefficient of thermal expansion (CTE) is calculated for the sintered samples between room temperature and 1000 °C, according to Mori et al. [12]. Values are $12.4 \cdot 10^{-6}$ K^{-1} for the as-sintered sample and $13.5 \cdot 10^{-6}$ K^{-1} for the reduced sample. The expansion rate of the reduced sample increases after 800 °C, indicating oxidation of the nickel in air. These CTE values are well within the expected values from Ref. [12], for our ratio of NiO vs YSZ.

The electrical conductivity of the sample will depend on the proportion of the different conducting phases as well as on the porosity fraction and can be estimated, in a first approximation, with the law of mixtures,

$$\sigma_{comp,1} = p_{Ni}\sigma_{Ni} + p_{YSZ}\sigma_{YSZ} + p_{pore}\sigma_{pore} \quad (1)$$

where σ_i represents the electrical conductivity of the composite and the various phases and p_i is the volume fraction of each phase in the sample ($p_{Ni} + p_{YSZ} + p_{pore} = 1$). The electrical conductivity of Ni and 8YSZ at 25 °C is equal to 146200 S cm^{-1} and 0.006 S cm^{-1}, respectively [13,14]. As the conductivity of the pore is assumed equal to zero, Eq. (1) can be rewritten as:

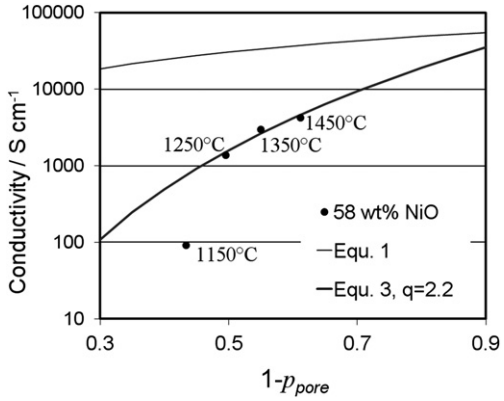

Fig. 4. Room temperature electrical conductivity versus the solid fraction ($1 - p_{pore}$) of the bar samples sintered at different temperatures (after reduction 12 h at 800 °C under H_2). The lines are based on the law of mixtures (Eq. (1)) and a power law model (Eq. (3)) with $q = 2.2$. See details in the text.

$$\sigma_{comp,1} = (1 - p_{pore})\sigma_{eff} \text{ with } \sigma_{eff} = \nu_{Ni}\sigma_{Ni} + \nu_{YSZ}\sigma_{YSZ} \quad (2)$$

where ν_{Ni} and ν_{YSZ} are the Ni and the YSZ volume fraction in the solid phase ($\nu_{Ni} + \nu_{YSZ} = 1$ and $1 - p_{pore} = p_{Ni}/\nu_{Ni} = p_{YSZ}/\nu_{YSZ}$).

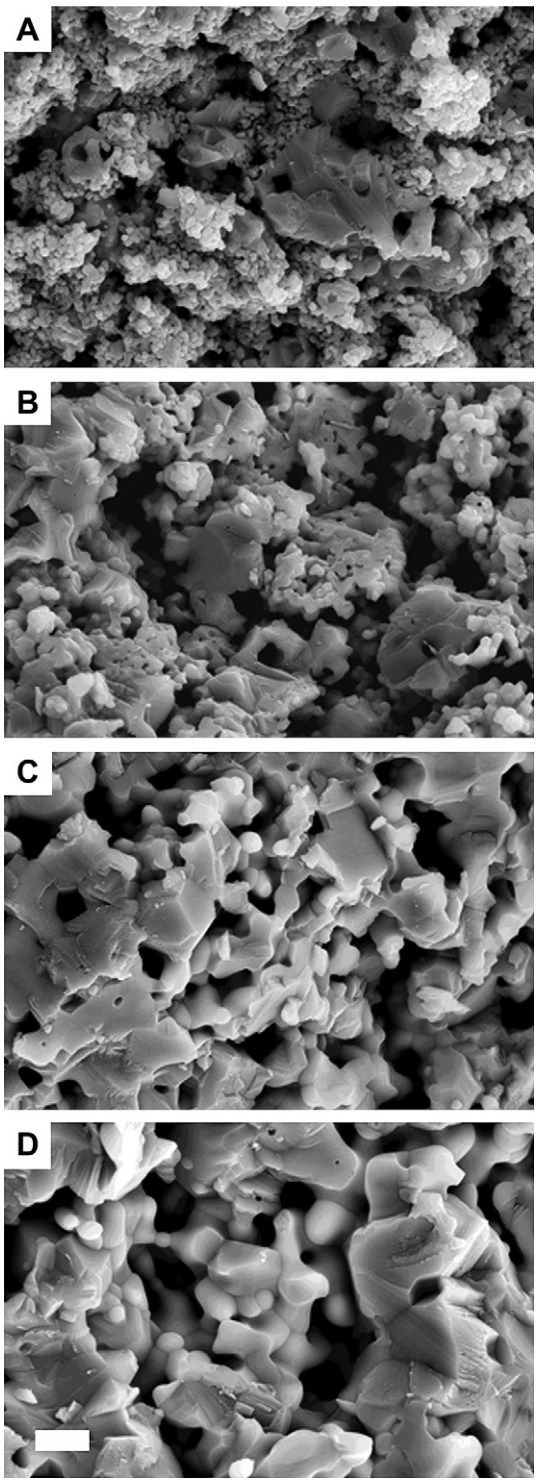

Fig. 5. Scanning electron micrographs of rupture surfaces of the injected bars, at 4 various sintering temperatures (A = 1150 °C, B = 1250 °C, C = 1350 °C and D = 1450 °C) in the as-sintered state. Scale bar in D is 2 μm and equal for all micrographs.

A different model includes a power law with an exponent depending on the conducting phase fraction (ν_{Ni}) and a fitting parameter, q [15]:

$$\sigma_{comp,2} = \left(1 - p_{pore}\right)^{\frac{q}{\nu_{Ni}}} \sigma_{eff} \quad (3)$$

Fig. 4 presents the electrical conductivity measured versus the solid fraction $(1 - p_{pore})$ of the reduced bar samples sintered at four different temperatures. It can be seen that the law of mixtures overestimates the measured electrical conductivity because the contact surface between the conducting particles is not taken into account (inducing current constriction) [16]. The best fit with the power model proposed in Eq. (3), for sintering temperatures between 1250 °C and 1450 °C, is obtained with $q = 2.2$. A previously published value of q was between 1.6 and 1.9 [15]. The slightly higher q value obtained in this work could be explained by the fact that the base powders, the fabrication process and the sintering temperatures are different from Ref. [15], as q is believed to depend on the microstructure

The conductivity of the sample sintered at 1150 °C does not follow the power law model. The microstructure comparison in Fig. 5 reveals that the zirconia powder is not sintered after one hour at 1150 °C. During NiO reduction (12 h at 800 °C under pure H_2), the nickel will reorganize and might agglomerate if the YSZ backbone is not sintered. It has been shown that this agglomeration can reduce the electrical conductivity [17,18].

The sequence of the thin cell layers is presented in Fig. 6. At the bottom of the SEM micrograph, the microstructure of the PIM anode-support in its reduced state after testing is clearly visible. The electrolyte layer is about 12 μm thick and the LSM–YSZ cathode between 5 and 10 μm (depending on the location). On top of the cathode, the LSC-based current collection layer can be seen. Some porosity remains in the YSZ electrolyte, but the pores seem to be closed.

The electrochemical performance at 810 °C is comparable to previous works on LSM–YSZ cathode [19] (see Fig. 7), even though the cathode thickness is here lower than usual and has therefore probably limited the output. The power density reaches 0.45 W cm^{-2} at 0.6 V. The current limitation at 1.15 A cm^{-2} is due to the AutoLab® measurement instrument. The relatively low open circuit voltage (OCV) is explained mainly by the setup design. Due to post-combustion of hydrogen at the edges of the cell, back-diffusion of steam decreases the OCV value. A similar OCV is also observed on 5 × 5 cm^2 tape-cast square cells [19], while values of

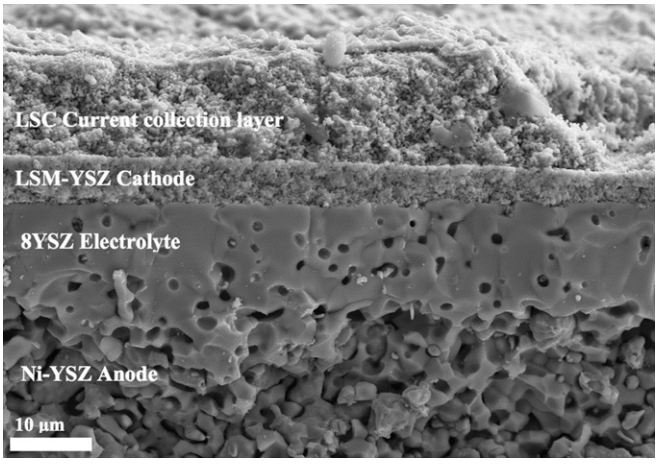

Fig. 6. Scanning electron micrograph of the tested cell in reduced state.

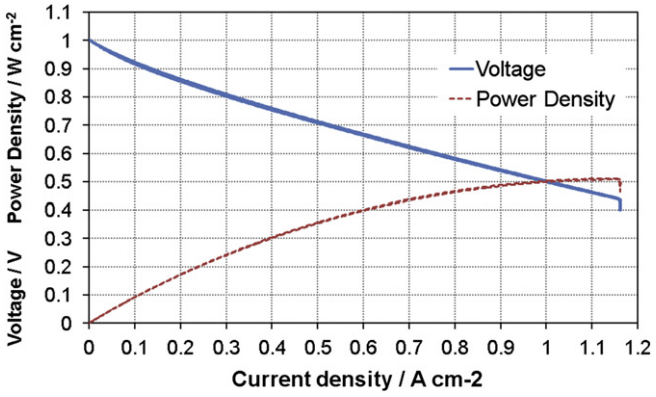

Fig. 7. Electrochemical characteristics (voltage and power density versus current density) of structured anode-supported SOFC fabricated by powder injection molding (PIM). Conditions: 810 °C, air = 450 ml min^{-1}, humidified hydrogen (3% H_2O) = 300 ml min^{-1}, time = 152 h.

1070 mV are attained with ø = 60 mm cells because of a reduced back-diffusion [20].

Despite the thickness of the injected anode (0.5 mm), no diffusion limitation is observed at high current densities.

The medium-term test shows a stable behavior of the cell in galvanostatic mode, initially at 670 °C and 0.1 A cm^{-2} during 150 h and then at 810 °C and 0.2 A cm^{-2} (see Fig. 8). After changing the temperature and the current density (time = 150 h), an activation of about 10 mV is observed during the next 50 h. Following this, the voltage decreases by about 5 mV during the next 500 h. A linear approximation of the voltage drop with time between 236 h and 698 h gives a value of −9.6 μV h^{-1}, equivalent to about 1.1% voltage degradation per 1000 h. A second potential rise of 15 mV is observed after 700 h during a very short period of 2 h followed by a degradation of −28.3 μV h^{-1} between 700 and 872 h. After 872 h, the test had to be shut down due to laboratory maintenance work.

The initial activation is probably due to the LSM cathode [21,22]. The second potential increase (700 h) is linked to premature termination of the fuel humidification (from 3% to a fraction <0.1%). It improved the OCV value and the performance of the cell, but the degradation rate increased when water feeding at the anode stopped inadvertently.

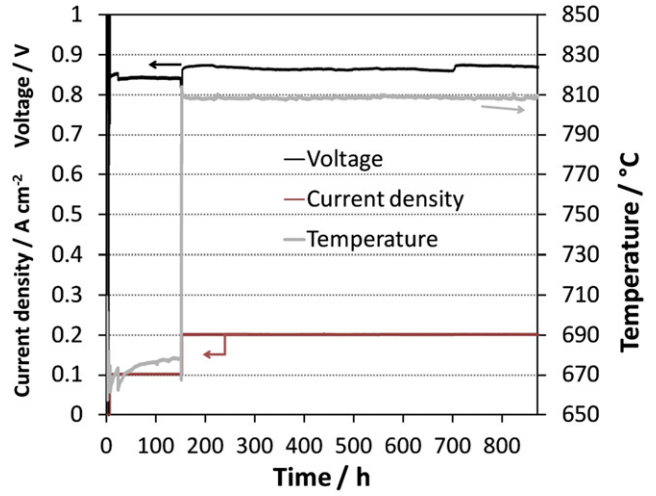

Fig. 8. Medium term galvanostatic electrochemical test of structured anode-supported SOFC fabricated by powder injection molding (PIM). Conditions: air = 450 ml min^{-1}, humidified hydrogen (3% H_2O) = 300 ml min^{-1}.

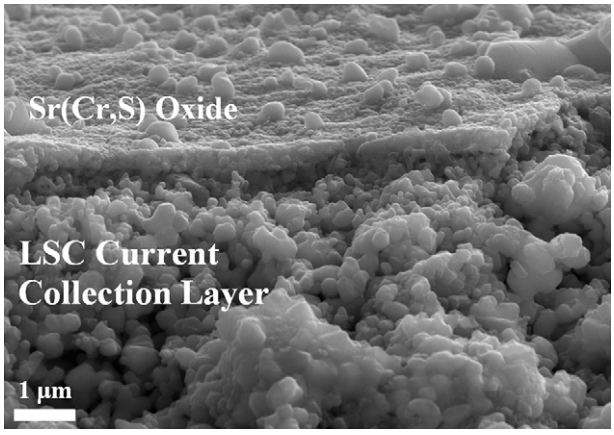

Fig. 9. Scanning electron micrograph of the surface of the LSC current collection layer. Energy dispersive X-ray spectrometry reveals Sr(Cr,S)-oxide phase on top.

Post-test observations (Fig. 9) show a rather dense cover layer on top of the LSC cathode current collecting layer. This layer is about half a micron thick and presents some crystalline structure. Energy dispersive X-ray spectrometry (EDS) gives a composition around 80 at% oxygen, 10 at% strontium, 8 at% chromium and 2 at% sulfur. This compound is a sulfur-containing strontium chromate and has already been observed before on top of the LSC layer [23–25]. The origin of the chromium is the high-temperature Ni-based alloy with >22 wt% Cr content (Inconel 602) used for air preheating tubes; a previous study showed Cr-poisoning of the SOFC cathode due to chromium evaporation from an Inconel 600 alloy [26]. Volatile chromium is known to react with LSC and form $SrCrO_4$, so only part of the Cr reaches the LSM interface [27]. The origin of sulfur is the compressed air feed with a concentration of about 10 ppb SO_2. A recent study demonstrated the combination of Cr and S poisoning of SOFC cathodes. Sr–Cr oxide compounds act as a getter for sulfur that occupies the B site producing a $Sr(Cr_{1-x},S_x)O_{4-d}$ phase [25].

This observation as well as our previous experience suggest that the main part of the degradation observed here can be attributed to the cathode pollution in the present test, indicating promising performance and stability potential for the anode fabricated by PIM.

4. Conclusions

This work reports on a feasibility study of anode-supported SOFCs produced by powder injection molding (PIM). Test bar samples have been sintered at four different temperatures between 1150 °C and 1450 °C. The residual porosity after sintering varies between 44% and 21% depending on the temperature and corresponds to the values needed for an SOFC anode-support. For samples sintered at and above 1250 °C, the room temperature electrical conductivity is well above 1000 S cm^{-1}.

The electrochemical performances of the structured anode-supported cell are comparable to those from thin tape-cast cells with LSM–YSZ cathode. The absence of noticeable diffusion limitations in the investigated case shows that a structured anode support produced by PIM can meet the operational requirements of a commercial SOFC. Future work on the electrodes will improve the cell performance.

The degradation test gives an approximate voltage decay of about 1.1% per 1000 h, which is comparable to similar tests on tape-cast cells, where it was attributed mainly to the cathode, due to chromium and sulfur poisoning. A similar degradation is probably occurring also in the present test, conferring promising potential to the PIM anode.

Acknowledgments

Kind acknowledgments are addressed to Arburg GmbH for their support and valuable discussions. Thanks are due to D. Zufferey for his help with the experiments and the SEM observations. This work has been made possible thanks to an HES-SO funding through an RCSO-MaCHoP project grant.

References

[1] R. Oberacker, Powder compaction by dry pressing, in: R. Riedel, I.-W. Chen (Eds.), Ceramics Science and Technology, Synthesis and Processing, vol. 3, Wiley-VCH Verlag GmbH & Co. KGaA, Weinheim, 2011, p. 532.
[2] T. Jardiel, M.E. Sotomayor, B. Levenfeld, A. Várez, Int. J. Appl. Ceram. Technol. 5 (2008) 574–581.
[3] G. Matula, T. Jardiel, B. Levenfeld, A. Varez, J. Achieve. Mater. Manuf. Eng. 36 (2009) 87–94.
[4] B. Arias-Serrano, T. Jardiel, G. Matula, A. Varez, B. Levenfeld, PM2010 World Congress – PM Functional Materials, Florence, Italy, 2010, pp. 313.
[5] A. Mirahmadi, S. Rezaee, EPJ Web Conf. 6 (2010).
[6] A. Panahi, H. Khoshkish, M. Saraji, Ionics 17 (2011) 733–740.
[7] J. Xiao, J. Liu, J. Ding, ECS Trans. 35 (2011) 609–614.
[8] A. Zryd, H. Girard, A. Faes, E. Carreno-Morelli, European Powder Metallurgy Congress EuroPM11, Barcelona, Spain, 2011, vol. 3, pp. 401–405.
[9] A. Faes, A. Zryd, H. Girard, E. Carreno-Morelli, Z. Wuillemin, J. Van herle, O. Bucheli, M. Spirig (Eds.) 10th European Solid Oxide Fuel Cell Forum, Lucerne, Switzerland, 2012, pp. A0702.
[10] M. Cologna, A.R. Contino, D. Montinaro, V.M. Sglavo, J. Power Sources 193 (2009) 80–85.
[11] P. Tanasini, M. Cannarozzo, P. Costamagna, A. Faes, J. Van Herle, A. Hessler-Wyser, C. Comninellis, Fuel Cells 9 (2009) 740–752.
[12] M. Mori, T. Yamamoto, H. Itoh, H. Inaba, H. Tagawa, J. Electrochem. Soc. 145 (1998) 1374–1381.
[13] D.W. Dees, T.D. Claar, T.E. Easler, D.C. Fee, F.C. Mrazek, J. Electrochem. Soc. l34 (1987) 2141–2146.
[14] R.M.C. Clemmer, S.F. Corbin, Solid State Ionics 180 (2009) 721–730.
[15] A. Faes, J.M. Fuerbringer, D. Mohamedi, A. Hessler-Wyser, G. Caboche, J. Van herle, J. Power Sources 196 (2011) 7058–7069.
[16] P. Costamagna, P. Costa, V. Antonucci, Electrochim. Acta 43 (1998) 375–394.
[17] D. Simwonis, F. Tietz, D. Stoever, Solid State Ionics 132 (2000) 241–251.
[18] A. Faes, A. Hessler-Wyser, D. Presvytes, C.G. Vayenas, J. Van herle, Fuel Cells 9 (2009) 841–851.
[19] D. Larrain, J. Van herle, F. Marechal, D. Favrat, J. Power Sources 118 (2003) 367–374.
[20] P. Tanasini, J.A. Schuler, Z. Wuillemin, M.L.B. Ameur, C. Comninellis, J. Van herle, J. Power Sources 196 (2011) 7097–7103.
[21] E. Siebert, A. Hammouche, M. Kleitz, Electrochim. Acta 40 (1995) 1741–1753.
[22] X.J. Chen, K.A. Khor, S.H. Chan, Solid State Ionics 167 (2004) 379–387.
[23] Z. Wuillemin, Experimental and modeling investigations on local performance and local degradation in solid oxide fuel cells, PhD thesis 4525, Laboratory of Industrial Energy Systems (LENI), Ecole Polytechnique Federale de Lausanne (EPFL), Lausanne, Switzerland, 2009.
[24] Z. Wuillemin, A. Nakajo, A. Mueller, J.A. Schuler, S. Diethelm, J. Van herle, D. Favrat, ECS Trans. 25 (2009) 467.
[25] J.A. Schuler, H. Yokokawa, C.F. Calderone, Q. Jeangros, Z. Wuillemin, A. Hessler-Wyser, J. Van herle, J. Power Sources 201 (2012) 112–120.
[26] S. Taniguchi, M. Kadowaki, H. Kawamura, T. Yasuo, Y. Akiyama, Y. Miyake, T. Saitoh, J. Power Sources 55 (1995) 73–79.
[27] H. Yokokawa, T. Horita, N. Sakai, K. Yamaji, M.E. Brito, Y.P. Xiong, H. Kishimoto, Solid State Ionics 177 (2006) 3193–3198.